High-order above-threshold ionization in stretched molecules

C. C. Chirilă and M. Lein

Max Planck Institute for Nuclear Physics, Saupfercheckweg 1, 69117 Heidelberg, Germany
and Institute of Physics and Center for Interdisciplinary Nanostructure Science and Technology (CINSaT), Universität Kassel, Heinrich-Plett-Straße 40, 34132 Kassel, Germany
(Received 12 May 2006; published 3 November 2006)

By numerical solution of the time-dependent Schrödinger equation, highly accurate electron spectra are calculated for strong-field ionization of a one-dimensional H_2^+ molecular ion at large internuclear distances. Compared to the atomic spectra, we find additional cutoffs at high electron energies. The classical model for ionization (simple-man's model) adapted to the molecular geometry predicts cutoffs up to $50U_p$, where U_p is the ponderomotive potential. The cutoffs correspond to various scattering scenarios of the tunneled electron from the molecular sites. For certain internuclear distances the agreement between the classical predictions and the numerical spectra is unsatisfactory. We propose a modified simple-man's model based on complex electron trajectories, allowing for electrons appearing in the continuum with nonzero initial velocity from the tunneling ionization process. Agreement of the resulting cutoffs with the numerical results is recovered.

PACS number(s): 42.50.Hz, 33.80.Rv

An atomic or molecular system irradiated by a sufficiently strong laser can be ionized in a tunneling process in which a free electron with nearly zero velocity emerges from the potential barrier formed by the binding potential and the laser electric field. After tunneling, the center of the electronic wave packet follows approximately a classical trajectory. This wave packet may or may not return to the place of its origin. An electron that returns to the core and scatters elastically (once or more than once) is termed a rescattered electron, while if it propagates directly to the detector, it is called a direct electron. Even if a complete description is achieved only quantum mechanically, many qualitative and to some extent quantitative features of the ionization spectrum can be understood using the well-known simple-man's (SM) model, a classical model for ionization. For atoms, the simple-man's model predicts a cutoff energy of $2U_p$ for direct electrons and $10U_p$ for rescattered electrons (see [1] and references therein). Here, $U_p = E_0^2/4\omega^2$ is the ponderomotive potential, i.e., the average kinetic energy of a free electron in a laser field with electric-field amplitude E_0 and frequency ω. Instead of scattering, a returning electronic wave packet can recombine with the ionic core, leading to the emission of an energetic photon. While the ionization process is commonly denominated above-threshold ionization (ATI), the latter process is known as harmonic generation. The corresponding simple-man's model for harmonic generation [2] predicts a cutoff for the photon energy equal to $3.17U_p + I_p$, where I_p is the ionization energy of the atom.

Compared to atoms, molecular systems have more complex geometries and extra degrees of freedom, such as vibration and rotation. Therefore, they promise new interesting features of the well-known processes of above-threshold ionization and harmonic generation. A while ago, it was predicted [3], based on the simple-man's model adapted to the molecular geometry, that for molecules with certain, very large internuclear distances there exists a harmonic-generation mechanism by electron transfer with a cutoff energy at $8U_p + I_p$. This is to be contrasted with the harmonic generation cutoff energy for atoms, which is much smaller. The required stretching of molecules has already been realized in recent experiments [5]. In that work, the molecular

dissociation process of H_2^+ was traced up to large values of the internuclear distance R using a pump-probe scheme.

In the present work, our aim is to investigate the influence of the molecular geometry on the above-threshold ionization spectra. In molecules, the energy of direct electrons has the same cutoff as in atoms, but for large enough internuclear distances, the electrons can scatter from molecular sites other than the one that they emerged from. In the context of ATI, it was found numerically [6] for a one-dimensional H_2^+ model that electrons with energies much higher than $10U_p$ appear for large internuclear separation, but no systematic explanation was given. A similar effect was found for electrons scattered from pairs of ions [7,8] in the context of plasma physics.

For harmonic generation by electron transfer, it is important that the electron be delocalized over the molecular sites [9]. However, in the high-order ATI process, there is no need for delocalization, but only for the presence of a scattering center.

For simplicity, let us consider a one-dimensional model of H_2^+ with internuclear distance R. One proton (A) is positioned at $-R/2$ and the other one (B) at $+R/2$. An electronic wave packet that tunnels into the continuum in the vicinity of A has several possibilities. In case A it moves toward the detector, without scattering on the molecular sites. The simple-man's model predicts a $2U_p$ cutoff for the energy at the detector. In case AA the electron returns to the same site from which it tunneled and rescatters elastically. The cutoff is the same as for the similar process in atoms, namely, $10U_p$. In case AB the electron is accelerated by the laser field toward B, where it scatters elastically and then moves to the detector. In case AAB the electron tunnels from A, rescatters elastically from A, then reaches B where it scatters again, and finally leaves the interaction region to the detector. In case ABA the electron tunnels from A, scatters elastically on site B, and returns to A, where it scatters again. The scattering from the molecular sites can continue indefinitely, but the efficiency of such multiple-scattering processes will eventually become negligible due to the spreading of the electronic wave packet. Figure 1 shows the cutoffs of the final energies at the detector for the processes AB, AAB, and ABA obtained
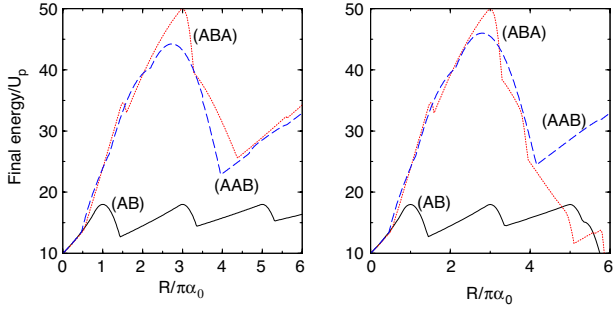
FIG. 1. (Color online) Predictions from the classical model for the maximal electron energies at the detector for the *AB*, *AAB*, and *ABA* scattering processes as a function of the internuclear separation (in units of $R_0 \equiv \pi\alpha_0$; see text). Left panel: monochromatic laser field. Right panel: a trapezoidal seven-cycle pulse.
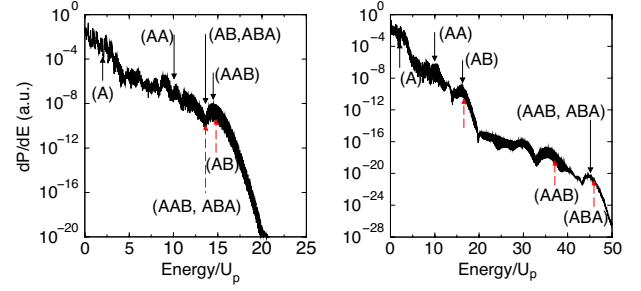

FIG. 2. (Color online) Above-threshold ionization spectra (see text for laser parameters). Different labels show the cutoffs predicted by the simple-man's model. The red (dashed) arrows show the corresponding cutoffs given by the CTSM model. Left panel: $R=0.5R_0$. Right panel: $R=2.5R_0$.

from the classical equations of motion, which we discuss in the following.

To formulate quantitatively the simple-man's model for these processes, let us denote by t_1 an arbitrary instant of time when the electron is detached from the nucleus *A* with initial velocity v_1. With $A(t) = -\int_{-\infty}^{t} E(t')dt'$ and $A_i \equiv A(t_i)$, the condition to reach *B* at time t_2 reads

$$R = \int_{t_1}^{t_2} [A(t) - A_1 + v_1]dt. \qquad (1)$$

After elastic backscattering from *B*, the velocity is $v(t) = A(t) - (2A_2 - A_1 + v_1)$, which gives the final kinetic energy at the detector for the *AB* process, $E_{AB} = (2A_2 - A_1 + v_1)^2/2$. For the second scattering, the electron needs to reach *A* again at time t_3:

$$R = -\int_{t_2}^{t_3} [A(t) - (2A_2 - A_1 + v_1)]dt. \qquad (2)$$

After backscattering from *A*, the kinetic energy at the detector is $E_{ABA} = (2A_3 - 2A_2 + A_1 - v_1)^2/2$. Equations (1) and (2) are used to find numerically the maximal energies for both a monochromatic laser field and a short laser pulse, as a function of the internuclear distance *R*. Similar equations apply to the *AAB* process. An initial velocity $v_1 = 0$ is assumed in all cases. The results are shown in Fig. 1.

The internuclear distance *R* is given in units of $R_0 = \pi\alpha_0$. We denote by $\alpha_0 = E_0/\omega^2$ the amplitude of oscillation of the free electron in the laser field. For an electron that is detached at *A* with zero initial kinetic energy to have maximal velocity at *B*, it has to start its motion when the electric field is zero and reach *B* after an odd number of half optical cycles. If it reaches *B* after one half cycle, the internuclear distance equals R_0. From the left panel of Fig. 1 (monochromatic field) one sees that the maximal cutoff for the *AB* process is $18U_p$ when *R* is an odd multiple of R_0 and for the *ABA* process the maximal cutoff is $50U_p$ when *R* is an odd multiple of $3R_0$. The *AAB* process is somewhat intermediate between *AB* and *ABA*. The maximal cutoff occurs at *R* $\approx 2.73R_0$ and is $\approx 44.2U_p$. For a short laser pulse, the results are shown in the right panel of Fig. 1. The laser electric field has a trapezoidal envelope, with two optical cycles of linear

turn-on and -off and three optical cycles of constant amplitude. The only difference with respect to the monochromatic case is that due to the finite duration of the laser pulse, an electron created at *A* does not have enough time to reach site *B* if the internuclear distance is too large.

The above scattering scenarios *AB* and *ABA* for high-order ATI are analogous to the ones discussed previously for high-harmonic generation [3]. The harmonic photon energies are maximal for the same values of the internuclear distance as found for the ATI electrons. For example, the maximal kinetic electron energy for recombination at site *B* after tunneling from *A* equals $8U_p$ [3,4].

In our quantum-mechanical simulation, the interaction of the electron with the two protons is modeled by the soft-core Coulomb potential $V(x) = -\{[(x-R/2)^2 + 1]^{-1/2} + [(x+R/2)^2 + 1]^{-/2}\}$. We solve the time-dependent Schrödinger equation in the length gauge with a laser pulse of 800 nm and intensity $I = 2 \times 10^{14}$ W/cm². For these laser parameters, the required internuclear distance for the maximal *AB* cutoff is $R_0 \approx 73$ a.u.

As we are interested in high-energy electrons, we use a large grid size of 1.3×10^4 a.u., with a spatial step $dr = 5 \times 10^{-2}$, while the time-propagation step is $dt = 5 \times 10^{-3}$. The grid has simple absorbing masks for the first and last 10% of its length, and it is large enough to avoid reflections from the boundaries for the wave packets with energies in the interval of interest, throughout the pulse duration. To reduce the computational time, we make use of the Crank-Nicolson scheme [10] with fourth-order accuracy in time [11] and space, which allows avoiding very small dt and dr. To achieve such high accuracy for the spatial derivatives and keep the tridiagonal structure for the numerical propagation, an implicit formula for the spatial derivative [12] was employed. The ionization spectrum is calculated accurately in a straightforward way by means of the window-operator method [13,14].

Figure 2 shows ATI spectra for two values of the internuclear distance. The black arrows denote the cutoffs predicted by the conventional simple-man's model. One can see that the predicted cutoff energies by the simple-man's model in Fig. 1 agree roughly with the cutoff positions in the ATI spectra. The complex-trajectory SM (CTSM) model proposed later in this work predicts the cutoffs shown by the red (dashed) arrows in the same picture. Although the CTSM
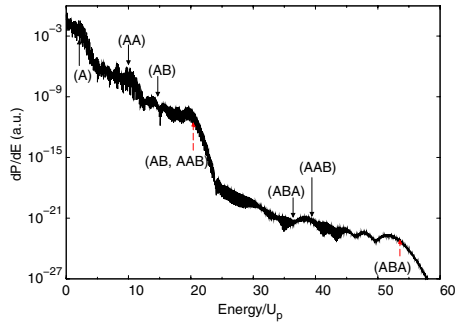
FIG. 3. (Color online) Above-threshold ionization spectra for $R=3.5R_0$. Different labels show the cutoffs predicted by the simple-man's model. The red (dashed) arrows show the corresponding cutoffs given by the CTSM model.

cutoffs for some processes agree with the conventional cutoffs given by the SM model, there are some differences, such as the AB and AAB cutoffs exchanging positions for $R=0.5R_0$, or AAB and ABA having cutoffs at different energies for $R=2.5R_0$. In the latter case, the cutoff of the AAB process agrees with the cutofflike structure visible in the ATI spectrum at the energy $\approx 37U_p$. For $R=0.5R_0$, the cutoffs for the AAB and ABA processes occur at almost the same energy, which coincides with a local minimum in the ATI spectrum. This may be explained by a possible destructive interference between trajectories belonging to both processes. Although the CTSM and SM predictions differ, the numerical results of Fig. 2 can be understood to a large extent within the simple SM model.

Disagreement with the simple-man's model is more striking for $R=3.5R_0$, shown in Fig. 3. The AB and ABA cutoffs underestimate the real cutoffs, while the predicted AAB cutoff has no corresponding cutoff in the ATI spectrum. In contrast, the CTSM model predicts the cutoffs accurately (red dashed arrows in Fig. 3). Agreement was obtained as well for all the other cases (not shown here) we looked at.

Thus, the conventional version of the simple-man's model does not reproduce correctly the cutoffs in the above-threshold ionization spectra for *all* internuclear distances. To this end, we propose a version that allows for nonzero initial velocities of the tunneled electron. Also, the electron is created in the continuum, not necessarily at A, but at a position similar to the out-of-the-barrier point in a simpler picture. In the spirit of the imaginary-time method [15], for a
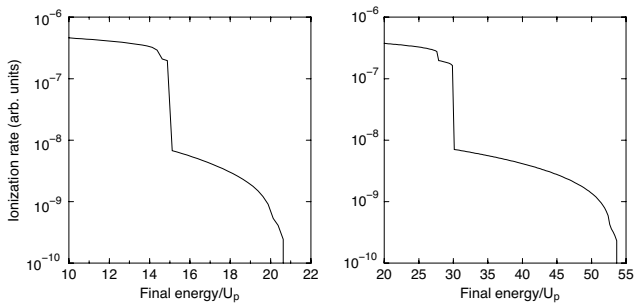
given creation time t_1 and initial velocity v_1, one can define an initial position x_1 where the tunneled wave packet appears in the continuum. Moreover, a rate can be assigned to the process, which will help later in assessing the contribution of a particular trajectory to the final ATI spectrum. The equations are rather intuitive. First, one finds the complex time t_s when the electron starts its trajectory from A (where it is most likely to be found) toward the exit from the tunnel. The condition that, moving under the influence of the field only, the electron has velocity v_1 at time t_1 and energy equal to the binding energy at the initial time t_s reads

$$\frac{[A(t_s) - A_1 + v_1]^2}{2} = -I_p. \qquad (3)$$

The electron dynamics for $t > t_1$ is described purely classically as in the SM model described before. From Eq. (3) only the solution t_s with positive imaginary part is chosen. In addition, to remove redundancy in the possible solutions we further require that $\mathrm{Re}(t_s)=t_1$. The initial position x_1 at time t_1 and the exponential factor w in the rate are given by

$$x_1 = \mathrm{Re}\left(\int_{t_s}^{t_1} [A(t) - A_1 + v_1] dt\right), \qquad (4)$$

$$\ln w \propto -2 \left| \mathrm{Im} \int_{t_s}^{t_1} \{[A(t) - A_1 + v_1]^2/2 + I_p\} dt \right|. \qquad (5)$$

Equation (5) contains only the tunneling process. For a more accurate prediction of the ATI signal, one would have to include the wave packet spreading together with the reflection coefficients of the wave packet on the molecular sites (see [8], where such a rate is calculated as a function of the kinetic energy of the incident wave packet).

When $R=0$, Eqs. (1), (3), and (5) are similar to the equations that describe the rescattering process in the framework of complex electron trajectories (see [16] and references therein). In that work, a similar set of equations, but not the same, are derived from the strong-field approximation model for ATI including rescattering. It would be interesting to see if the two approaches predict the same cutoff of the rescattering energy in atoms.

To gain more understanding of the CTSM model, in Fig. 4 we plot for both AB and ABA scattering processes ($R=3.5R_0$) the maximal tunneling rate as a function of the final kinetic energy. One can see that the energy has cutoffs in agreement with the time-dependent Schrödinger equation result shown in Fig. 3. The plots showing the ionization rates suggest that the cutoff energy should be taken as the last energy in the corresponding graph after which the rate drops dramatically. The results for the cutoffs are significantly different from those of the simple-man's model (see Fig. 3). This is to be expected due to both the nonzero velocities and the nonzero initial detachment position of the electron. This initial position x_1 from Eq. (4) can attain values comparable to α_0, as Fig. 5 shows. Also, from the same figure, one sees that the simple estimate of the exit position from the tunnel, $x_1 \approx -I_p/E(t_1)$, is valid at high electric fields and in the tunneling regime ($\gamma < 1$, where $\gamma = \sqrt{I_p/2U_p}$ is the Keldysh parameter). For a monochromatic field, analytical expressions can be obtained: $x_1[E(t_1)=0]=-\gamma\alpha_0$ and

FIG. 4. Left panel AB: The maximal ionization rate w [Eq. (5)] for a given final energy. Right panel: same as the left panel, but for the ABA process. The internuclear distance is $R=3.5R_0$.
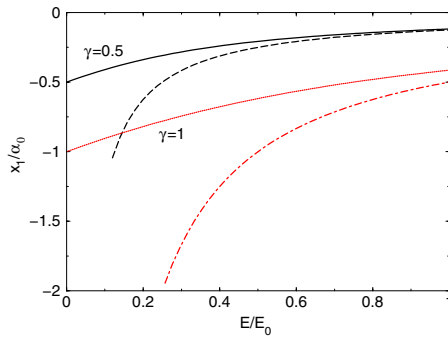
FIG. 5. (Color online) The detachment position x_1 as a function of the electric field at time of detachment. The field is monochromatic. Two values of the Keldysh parameter are considered. The dashed and the dot-dashed curve that approach the full and the dotted curve, respectively, at maximum field show the position given by the simple expression $x_1 = -I_p/E(t_1)$.

$x_1[E(t_1) = E_0] = \alpha_0(1 - \sqrt{\gamma^2 + 1})$. When the electric field $E(t_1)$ is negative, the exit position changes sign.

Finally, Fig. 6 shows in a manner similar to Fig. 4 the maximal ionization rates as a function of the final kinetic energy, for a range of internuclear distances R. The figure gives a visual impression as to how the cutoff energies vary as a function of the internuclear distance, in comparison to Fig. 1 from the simple-man's model.

In conclusion, we calculated the ATI spectra for a one-dimensional H_2^+ molecular ion, for various internuclear separations. We used the window-operator method to obtain the spectra and a high-order Crank-Nicolson algorithm for integrating the Schrödinger equation. The spectra show rich structures, in contrast to the simpler spectra for atoms. Various plateaus appear at high electron energies, much higher than the usual $10U_p$ cutoff for atoms. In general, these plateaus can be understood in the framework of the simple-man's model, adapted to the molecular geometry. For some values of the internuclear separation, however, the predictions of the SM model do not agree with the features present in the calculated spectra. We propose the complex-trajectory simple-man's model, which is an intuitive extension of the SM model. The CTSM is able to describe accurately the cutofflike features for all internuclear distances. This model allows for nonzero starting position and velocity for the continuum electron and therefore provides a physical
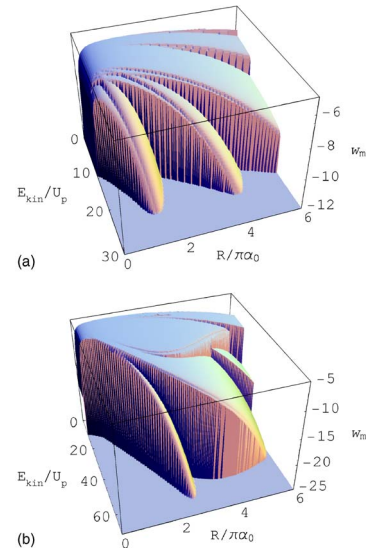

FIG. 6. (Color online) The maximal ionization rate w_m for a given final kinetic energy, as a function of the internuclear distance. Upper panel: the AB process; lower panel: the ABA process.

explanation of some unexpected features in the ATI spectra.

Already the classical explanation of the atomic cutoff at $10U_p$ [1] did not require Coulomb effects. For the high-order ATI cutoffs described in this work, we have ruled out the importance of Coulomb effects by comparing with numerical spectra we obtained for shorter-range potentials. They exhibit cutoffs at the same energies as in the Coulomb case.

Experimentally, it will be hard to observe the high-energy cutoffs near $50U_p$ because of the very low ionization yield. Nevertheless, Fig. 2 suggests that it should be possible to observe the predicted extension of the ATI spectrum beyond the $10U_p$ cutoff. The scattering mechanism could thus provide an interesting method to probe molecular dissociation at large internuclear separations. We stress that the electron delocalization as in the corresponding harmonic-generation process [9] is not needed here. We have confirmed this statement with test calculations where the initial state of the electron is localized to one site.

[1] G. G. Paulus *et al.*, J. Phys. B **27**, L703 (1994).

[2] P. B. Corkum, Phys. Rev. Lett. **71**, 1994 (1993).

[3] P. Moreno *et al.*, J. Opt. Soc. Am. B **13**, 430 (1996); Phys. Rev. A **55**, R1593 (1997); A. D. Bandrauk *et al.*, *ibid.* **56**, R2537 (1997); R. Kopold *et al.*, *ibid.* **58**, 4022 (1998).

[4] M. Lein and J. M. Rost, Phys. Rev. Lett. **91**, 243901 (2003).

[5] Th. Ergler *et al.*, Phys. Rev. Lett. **95**, 093001 (2005).

[6] S. Chelkowski and A. D. Bandrauk, Laser Phys. **7**, 797 (1997).

[7] J. Görlinger *et al.*, Laser Phys. **15**, 245 (2005).

[8] H.-J. Kull and V. T. Tikhonchuk, Phys. Plasmas **12**, 063301 (2005).

[9] M. Lein, Phys. Rev. A **72**, 053816 (2005).

[10] J. Crank and P. Nicolson, Proc. Cambridge Philos. Soc. **43**, 50 (1947).

[11] I. V. Puzynin *et al.*, Comput. Phys. Commun. **123**, 1 (1999); **126**, 158 (2000).

[12] H. G. Muller, Laser Phys. **9**, 138 (1999).

[13] K. J. Schafer and K. C. Kulander, Phys. Rev. A **42**, 5794 (1990); K. J. Schafer, Comput. Phys. Commun. **63**, 427 (1991).

[14] D. Bauer, Phys. Rev. Lett. **94**, 113001 (2005).

[15] V. S. Popov, Phys. At. Nucl. **68**, 686 (2005).

[16] D. B. Milošević *et al.*, Phys. Rev. A **71**, 061404(R) (2005).